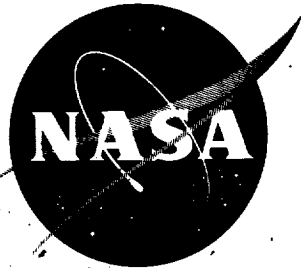


N63-10800

CODE 1

NASA TN D-1554



TECHNICAL NOTE

D-1554

LOCAL PRESSURE DISTRIBUTION ON A BLUNT DELTA WING

FOR ANGLES OF ATTACK UP TO 35° AT MACH

NUMBERS OF 3.4 AND 4.7

By Marvin Kussoy

Ames Research Center
Moffett Field, Calif.

NATIONAL AERONAUTICS AND SPACE ADMINISTRATION
WASHINGTON

December 1962



NATIONAL AERONAUTICS AND SPACE ADMINISTRATION

TECHNICAL NOTE D-1554

LOCAL PRESSURE DISTRIBUTION ON A BLUNT DELTA WING

FOR ANGLES OF ATTACK UP TO 35° AT MACH

NUMBERS OF 3.4 AND 4.7

By Marvin Kussoy

SUMMARY

The pressures on the windward surface of a delta wing, consisting of an elliptic paraboloid nose section and an elliptic cone afterbody, were investigated in air at Mach numbers of 3.4 and 4.7 and angles of attack up to 35° . The pressures obtained were compared with the predictions of two simple methods. In general, these methods bracketed the data, with the modified Newtonian flow and equivalent cone methods predicting pressures that were, respectively, lower and higher than those observed.

INTRODUCTION

Great interest has been shown in the use of blunt delta wings for lifting surfaces on hypersonic aircraft or reentry vehicles. For the latter vehicles reentry would be made at large angles to alleviate the high aerodynamic heating encountered and then the angle would be reduced and the lifting surfaces would permit control of the flight path.

Pressures have been measured on blunt flat-plate delta wings (e.g., refs. 1 and 2) and on elliptic cones (e.g., ref. 3). However, there are no pressure data available for the practical intermediate case of blunt elliptic cones. The effects of cone bluntness have been investigated for right circular cones (ref. 4). To supplement the existing data a wind-tunnel investigation has been conducted to measure the distribution of local pressure on a blunt delta wing with an elliptical cross section at supersonic Mach numbers, and over a large range of angles of attack. Comparisons have been made with some of the more simple methods for predicting local pressures on blunt lifting bodies, and the results are reported herein.

SYMBOLS

C_p pressure coefficient

M Mach number

p	pressure, lb/sq ft (unless otherwise stated)
Re	Reynolds number
s	arc length measured along body surface from leading edge, ft
T	temperature, $^{\circ}$ R
x, y, z	Cartesian coordinates, in.
α	angle of attack, deg
η	angle between the velocity vector and vector normal to the surface, deg
θ	peripheral angle, deg
Λ	sweepback angle, angle between the leading edge and a line perpendicular to the free-stream direction, deg

Subscripts

max	maximum
t	total conditions
∞	undisturbed free-stream conditions

EXPERIMENTAL APPARATUS AND PROCEDURES

Test Body

The shape of the test body is shown in figure 1. The surface between the planes $x = 0$ and $x = 1.4$ inches is an elliptic paraboloid described by the equation

$$y^2 + \frac{z^2}{(0.5)^2} = 0.4018x \quad (1)$$

Between the planes $x = 1.4$ and $x = 4.2$ inches, the surface is an elliptic cone with the vertex at $x = -1.4$ inches, and is described by the equation

$$\frac{y^2(13.93)}{(x + 1.4)^2} + \frac{z^2(55.76)}{(x + 1.4)^2} = 1 \quad (2)$$

The slopes along the surface were matched at $x = 1.4$ inches, and the sweepback angle Λ was 75° for $x > 1.4$ inches.

The test body was an electro-formed nickel shell with a nominal thickness of 0.015 inch. Pressure orifices, located as shown in table I, were used to measure the pressure distribution over the windward surface of this body. Each orifice was $1/64$ inch in diameter.

Test Conditions

All tests were carried out in the Ames 10-Inch Heat Transfer Wind Tunnel described in reference 5. The test body was sting-mounted from a side supported strut, which permitted rotation about a line passing through the chord plane at $x = 2.1$ inches. An examination of the data, and schlieren and shadowgraph pictures indicated that the strut did not interfere with flow over the test body.

Data were taken at Mach numbers of 3.4 and 4.7 and at various pressure levels. The tunnel conditions at which data were obtained are given in table II.

DATA REDUCTION

The free-stream static pressure measured at the side wall of the test section was used in evaluating the pressure coefficients. Previous tests in the tunnel indicated that the static pressure was constant across the test stream.

The data were repeatable within $\pm 2\%$ in pressure coefficient. This error was due to inaccuracies in reading the manometer tubes, setting the angle of attack, and positioning the test body on the sting.

METHODS OF PREDICTING SURFACE PRESSURES

To correlate the data obtained on the test body, two pressure prediction methods were investigated. The following is a brief description of these methods, together with the assumptions needed to apply them.

Newtonian Flow

Newtonian flow theory, described in reference 6, states that when a fluid stream impinges on an inclined surface, only its momentum component

normal to the surface is converted to a pressure force. Thus, bow-shock waves are ignored, and the pressure coefficient for Newtonian flow depends upon surface inclination only and is given by the equation

$$C_p = 2 \cos^2 \eta \quad (3)$$

where η is the angle between the velocity vector and a vector normal to the surface. If the given three-dimensional body is represented by the equation $f(x, y, z) = 0$, then

$$\cos \eta = \frac{\frac{\partial f}{\partial x} \cos \alpha + \frac{\partial f}{\partial z} \sin \alpha}{\sqrt{\left(\frac{\partial f}{\partial x}\right)^2 + \left(\frac{\partial f}{\partial y}\right)^2 + \left(\frac{\partial f}{\partial z}\right)^2}} \quad (4)$$

Since the pressure coefficient in equation (3) does not agree well with the isentropic flow value at the stagnation point, the modified form of equation (3) was used to give better over-all agreement. The modified form is

$$C_p = 1.8 \cos^2 \eta \quad (5)$$

Equivalent Cone

This method is presented and discussed in reference 3. It assumes that the local pressure at any point on a three-dimensional body is equal to that on the pointed circular cone (at $\alpha = 0^\circ$) whose surface has the same inclination to the free-stream velocity vector as the local point on the given body. By means of the inclination angle η and chart 6 of reference 7, the pressure coefficient can readily be determined.

RESULTS AND DISCUSSION

Measurements of Surface Pressures

Since the pressure measurements were made on the windward surface only, the following discussion pertains only to that surface. These measurements are presented in figure 2 for the windward surface, and in figure 3 for the most windward streamline. For simplicity of presentation, the pressure data are arbitrarily identified as being obtained on only one side of the most windward streamline. This is permissible, since the test body and air stream are symmetrical and all tests were made without sideslip. Furthermore, the different Reynolds numbers for the two sets of data at each Mach number (table II) are not indicated on these figures because there were no significant effects of Reynolds number.

From figure 2 it can be seen that at 0° angle of attack, C_p is higher along the leading-edge line and decreases toward the center line of the body. As the angle of attack is increased, C_p decreases along the leading edge but increases toward the center of the body. This is what one would expect as a result of the inclination of the windward surface and leading-edge line to the flow direction. The pressure coefficient is essentially constant at any angle of attack between peripheral angles of 90° and 40° .

From the data presented in figure 3 along the most windward streamline, it is seen that the pressures are high in the nose region, but decrease rapidly to an approximately constant value in the aft portion of the body for all angles of attack. The level of C_p increases with increasing angle of attack because of the increased surface inclination. Since the pressure tap at $s/s_{max} = 0$ is no longer the stagnation point at angles of attack other than zero, the pressure at this point decreases as the angle of attack is increased.

Both figures 2 and 3 show that the pressure coefficient was independent of Mach number for the small range of this parameter investigated in the tests.

Comparison of Measured and Calculated Surface Pressures

The pressure distributions predicted by the two methods discussed previously are also presented in figures 2 and 3. In general, these methods bracket the data, with modified Newtonian flow predicting values that are somewhat lower than the measurements, and the equivalent cone method giving values generally higher than measured pressures.

Ames Research Center
National Aeronautics and Space Administration
Moffett Field, Calif., Aug. 21, 1962

REFERENCES

1. Bogdonoff, Seymour M., and Vas, I. E.: An Exploratory Study of a Delta Wing at Hypersonic Speeds. Part II - Further Detailed Studies of the Pressure Distribution at Angles of Attack: 60° Included Angle Delta With a Blunted Edge. Air Research and Development Command TR 57-50, 1956.
2. Betram, Mitchell H., and Henderson, Arthur, Jr.: Recent Hypersonic Studies of Wings and Bodies. ARS Journal, vol. 31, Aug. 1961, pp. 1129-1139.
3. Zakkay, Victor: An Investigation of the Pressure Distribution on Conical Bodies in Hypersonic Flows. Jour. Aero. Sci., vol. 26, July 1959, p. 457.
4. Amick, James L.: Pressure Measurements on Sharp and Blunt 5° and 15° Half Angle Cones at Mach Number 3.86 and Angles of Attack to 100°. NASA TN D-753, 1961.
5. Tendeland, Thorval: Effects of Mach Number and Wall-Temperature Ratio on Turbulent Heat Transfer at Mach Numbers From 3 to 5. NASA TR R-16, 1959.
6. Seaman, Donna Jean, and Dore, Frank J.: Force and Pressure Coefficients of Elliptic Cones and Cylinders in Newtonian Flow. Consolidated Vultee Aircraft Corp., San Diego Division, Rep. ZA-7-004, 1952.
7. Ames Research Staff: Equations, Tables and Charts for Compressible Flow. NACA Rep. 1135, 1953.

TABLE I.- INSTRUMENTATION ON TEST BODY

Pressure Taps

x, in.	θ , deg	s/s _{max}
0	--	0
.25	90.0	.061
.50	0.0	--
.50	38.3	--
.50	90.0	.130
.75	90.0	.191
1.00	90.0	.252
1.50	19.8	--
1.50	90.0	.368
1.50	180.0	--
2.00	90.0	.486
2.50	0.0	--
2.50	42.5	--
2.50	90.0	.603
2.50	119.1	--
2.50	161.6	--
2.50	180.0	--
3.00	90.0	.721
3.50	19.1	
3.50	41.3	
3.50	90.0	.837
3.50	180.0	--

TABLE II.- TUNNEL OPERATING CONDITIONS

Condition	M _∞	p _{t_∞} , in. Hg abs	T _{t_∞} , °R	α , deg	Re _∞ per ft
1	3.4	93	710	0,15,25,35	3.88×10^6
2	3.4	142	710	0,15,25,35	5.93×10^6
3	4.7	142	710	0,15,25	3.21×10^6
4	4.7	176	710	0,15,25	3.98×10^6

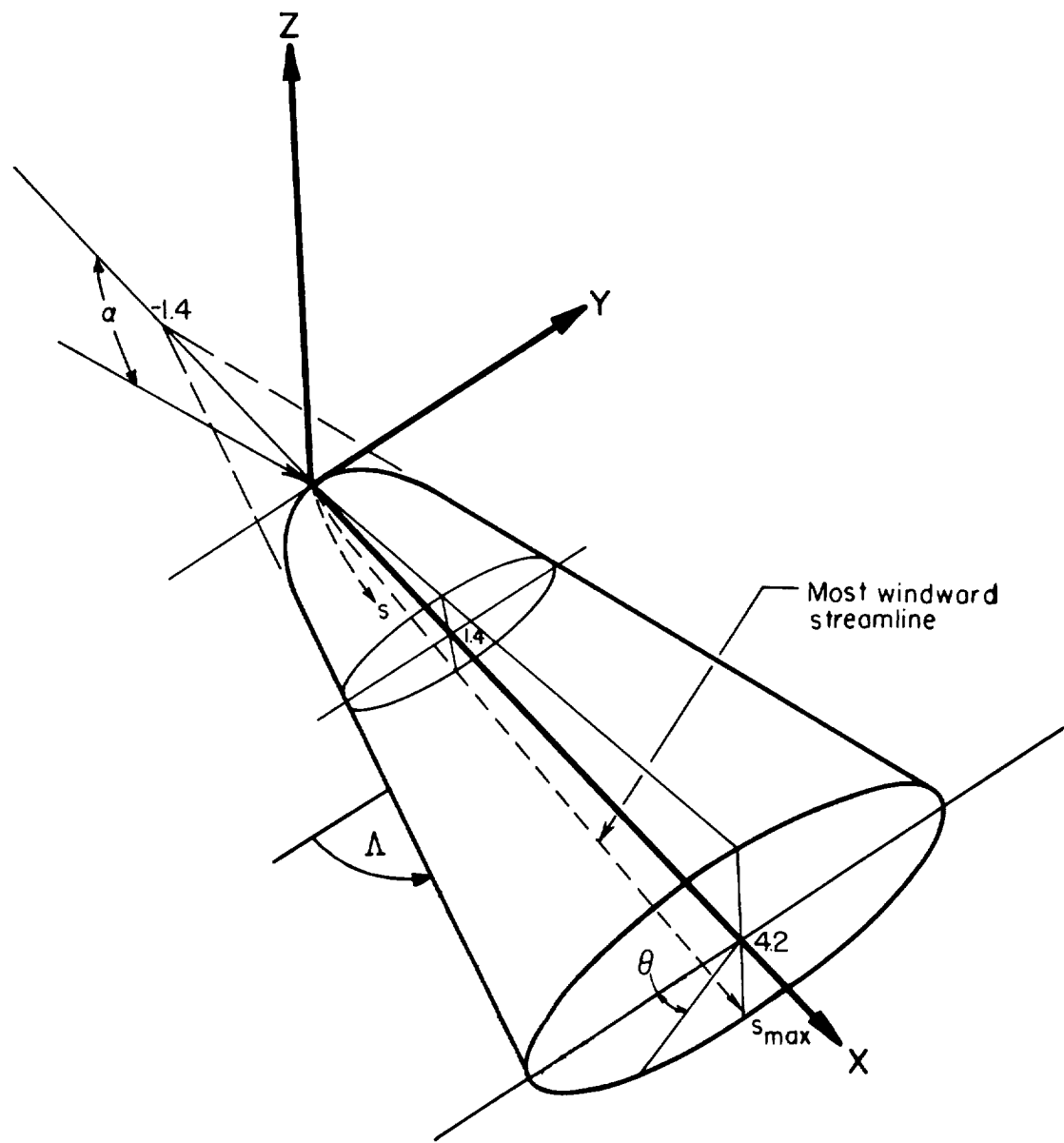


Figure 1.- Sketch of body.

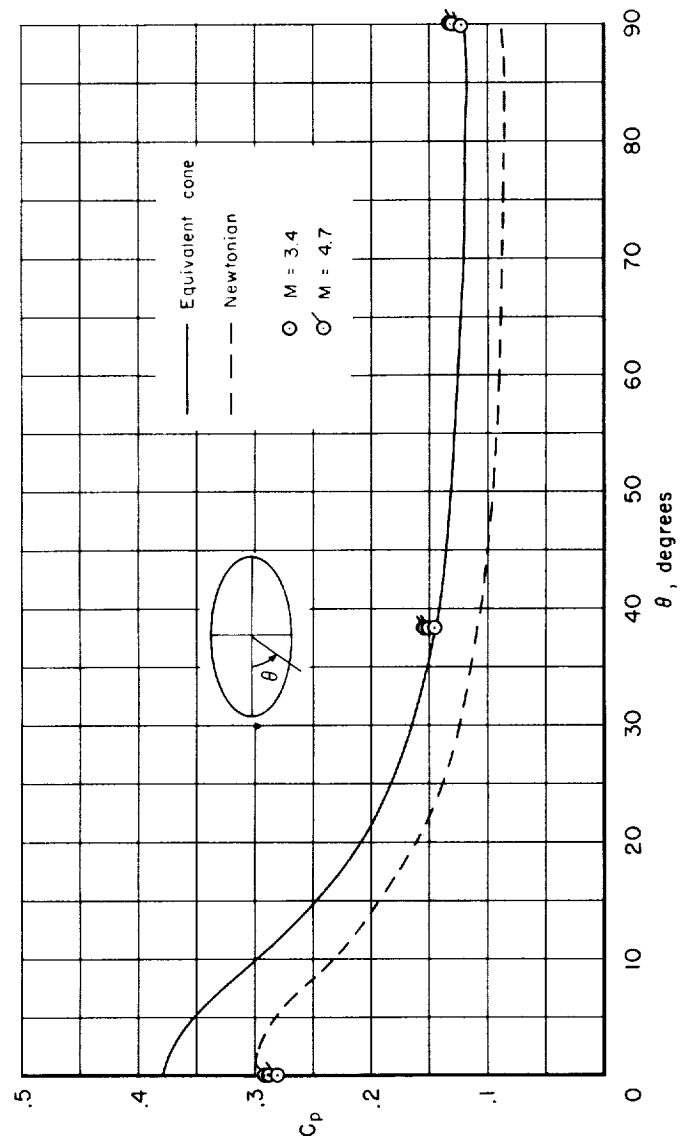


Figure 2.- Local static-pressure distribution on windward surface.
 (a) $x = 0.5$, $\alpha = 0^\circ$

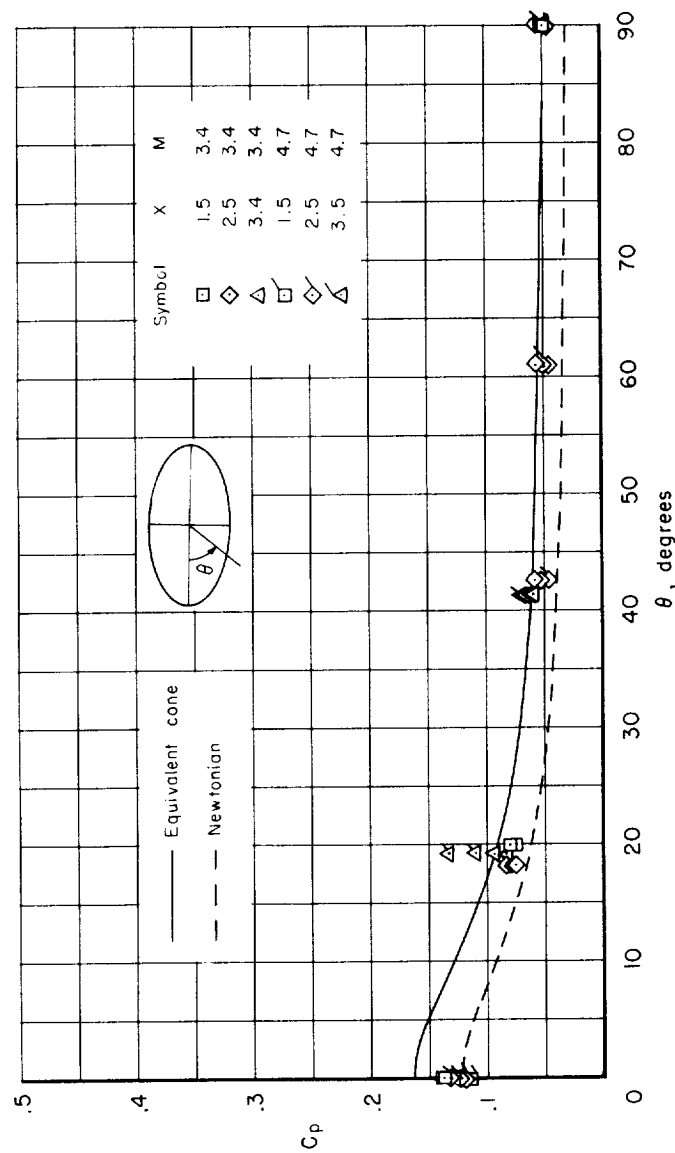
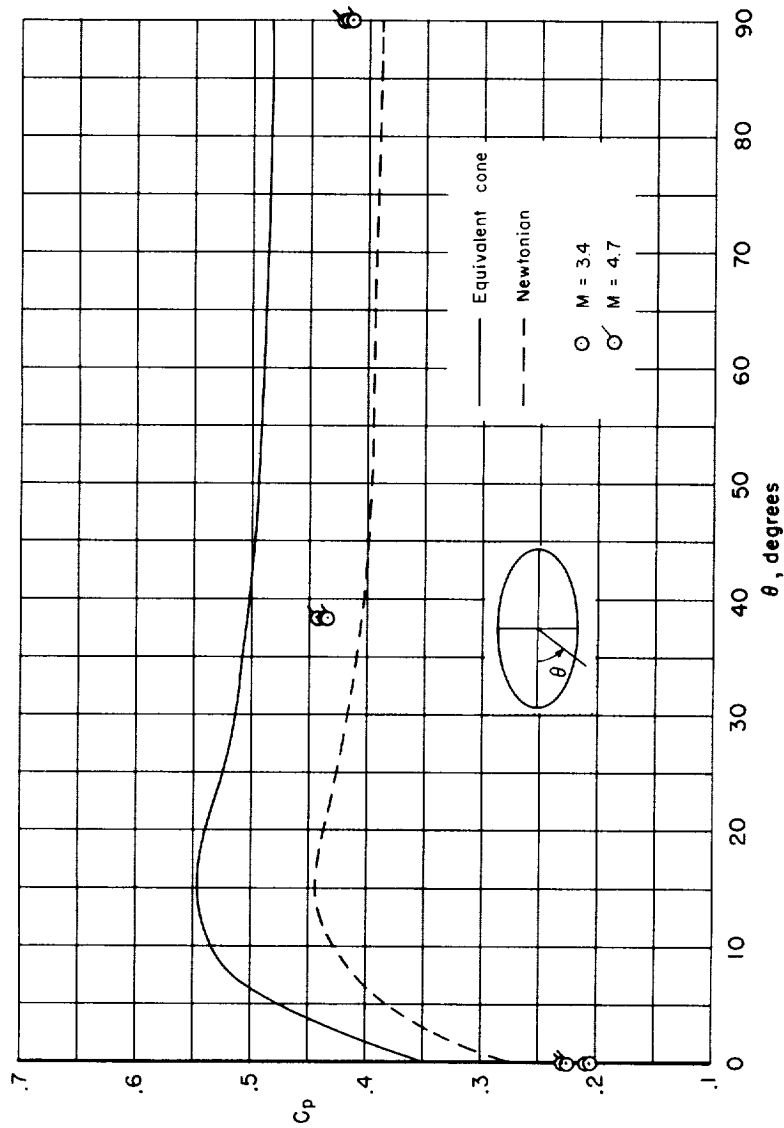
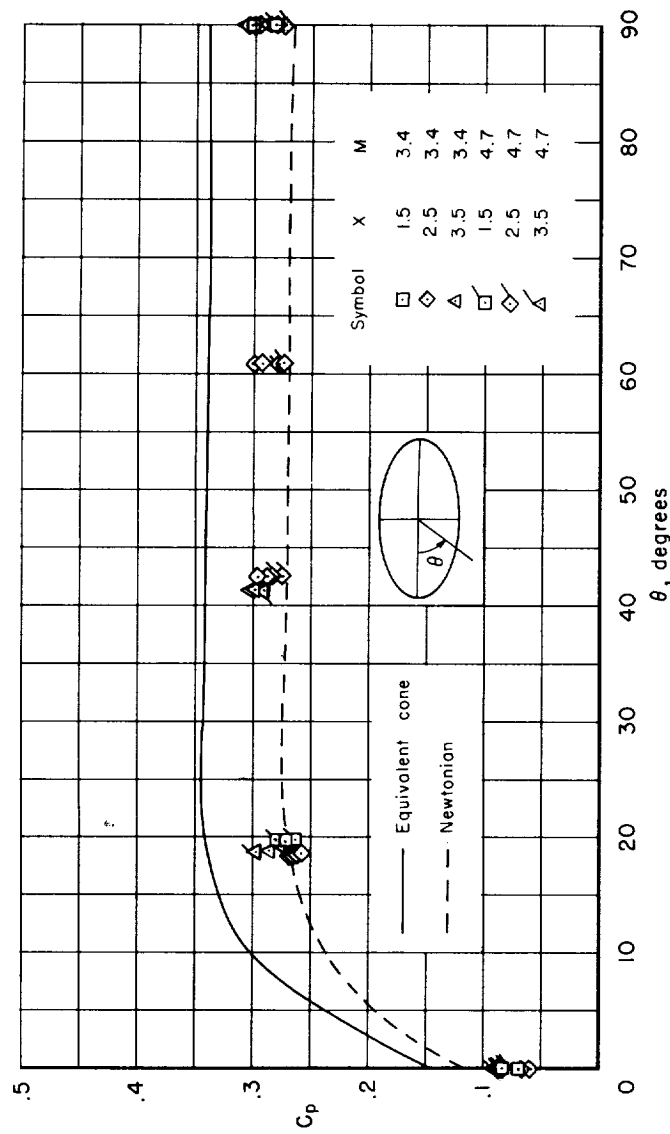
(b) $x > 1.4$, $\alpha = 0^\circ$

Figure 2.- Continued.



(c) $x = 0.5, \alpha = 15^\circ$

Figure 2.- Continued.



(d) $\chi > 1.4$, $\alpha = 15^\circ$

Figure 2.- Continued.

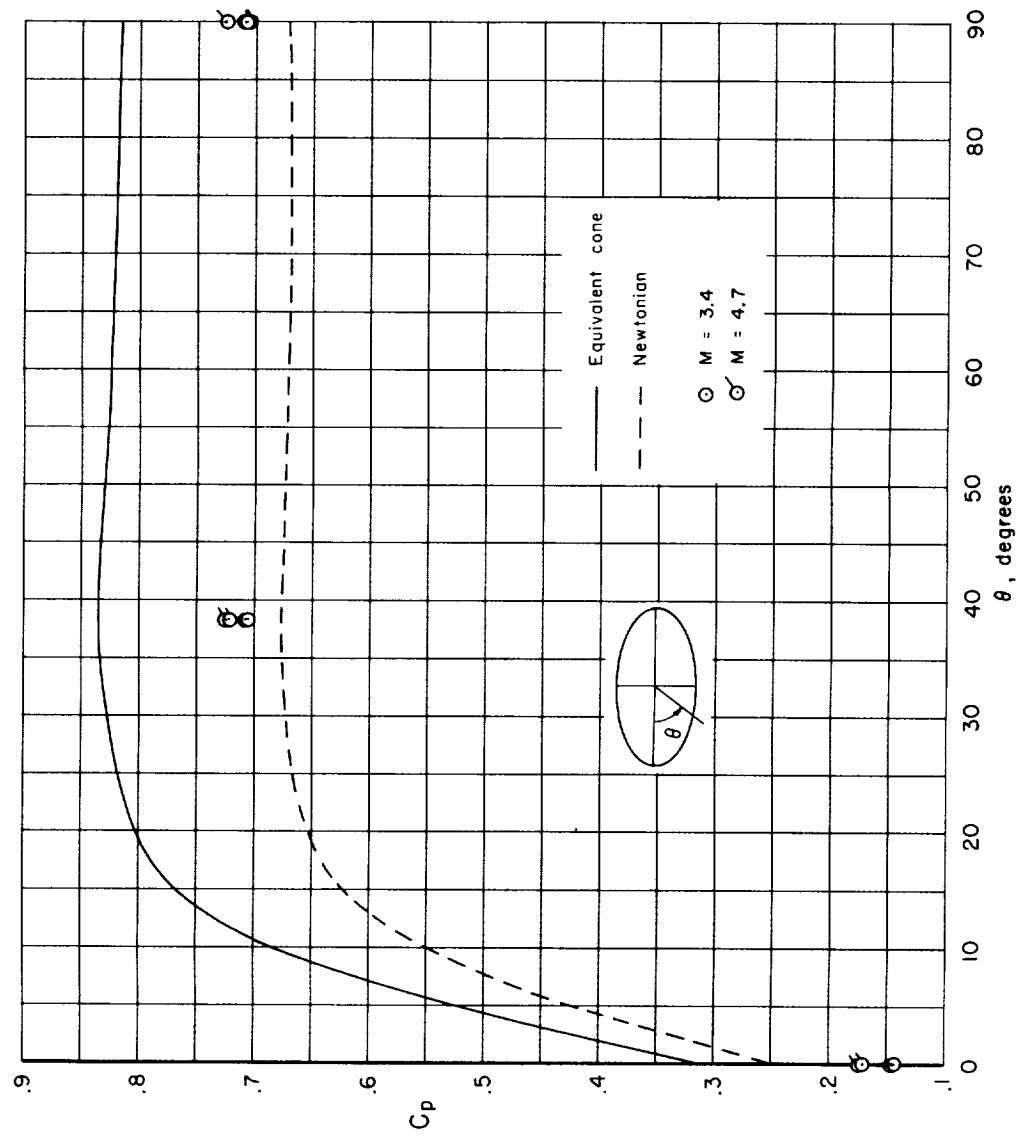
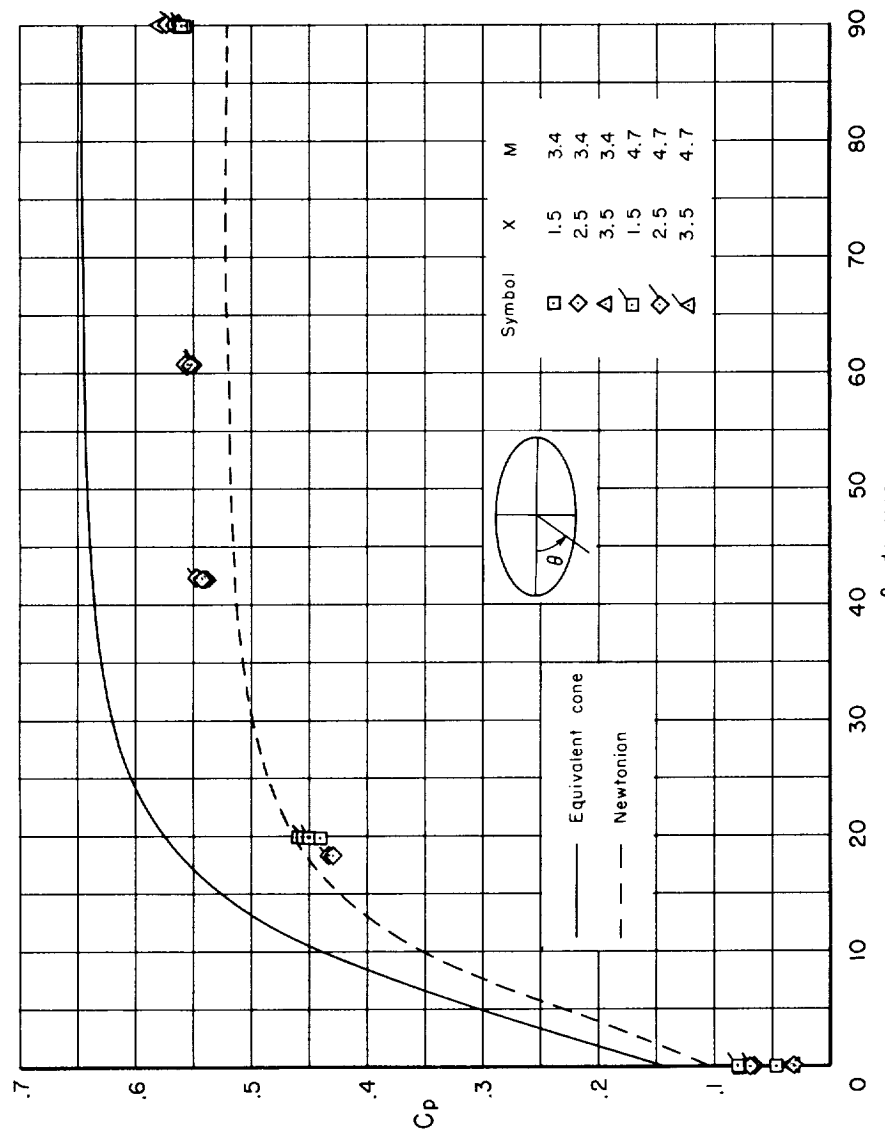
(e) $x = 0.5$, $\alpha = 25^\circ$

Figure 2.- Continued.



(f) $X > 1.4$, $\alpha = 25^\circ$

Figure 2.- Continued.

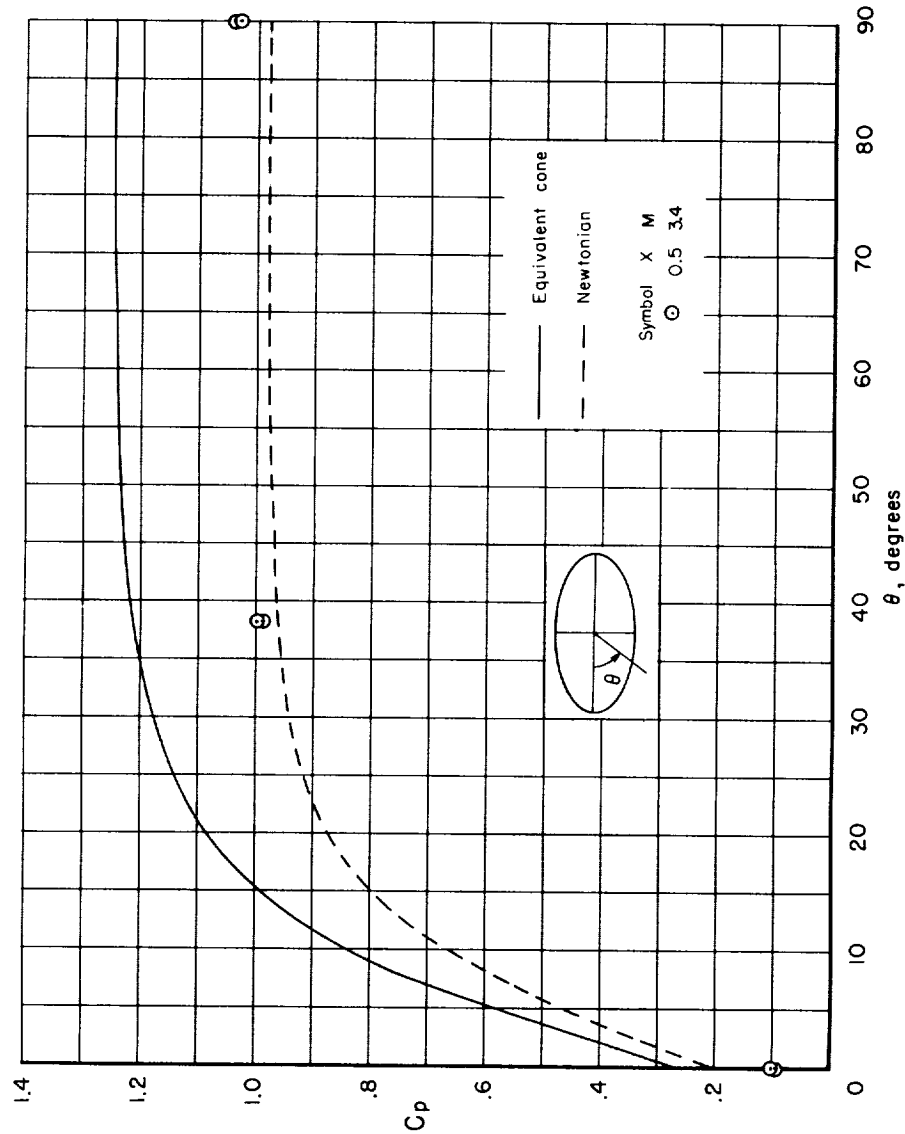
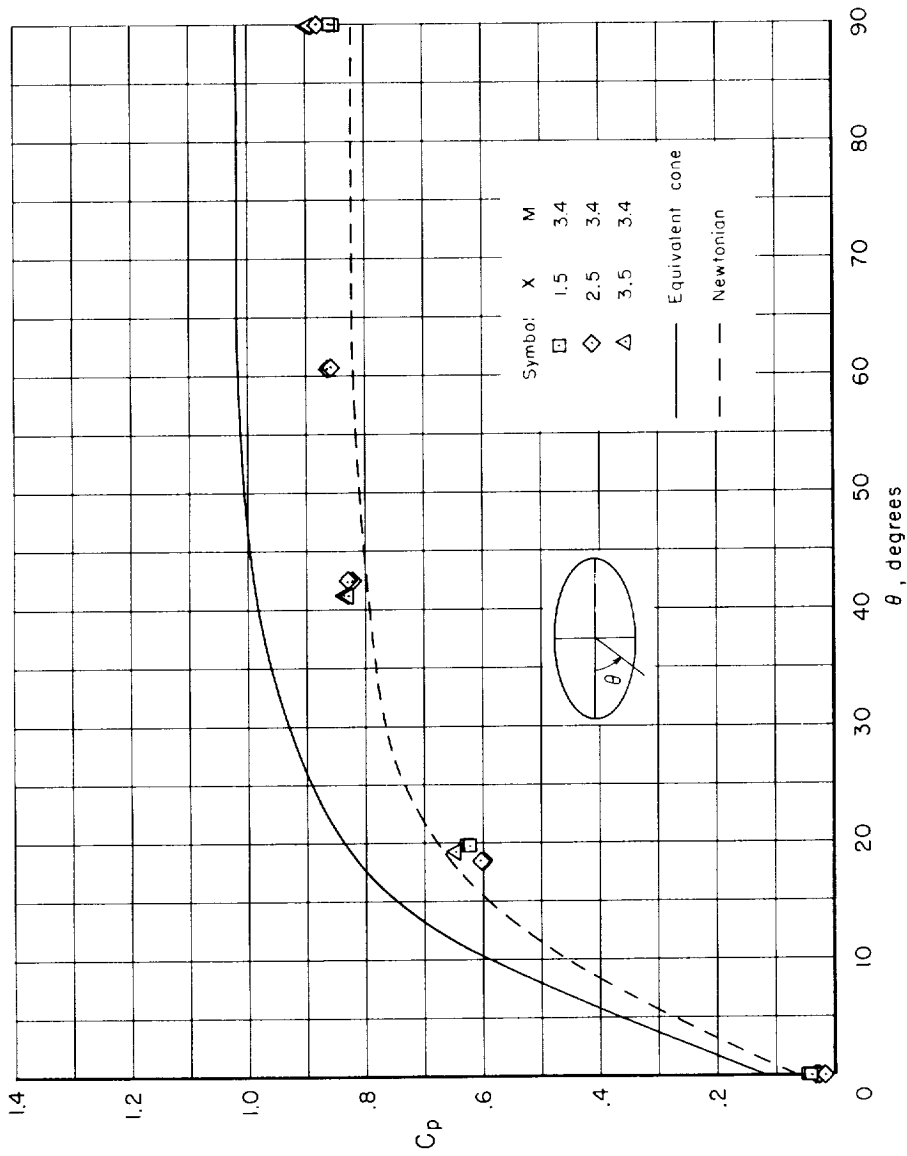
(e) $x = 0.5$, $\alpha = 35^\circ$

Figure 2.- Continued.



(h) $x > 1.4, \alpha = 35^\circ$

Figure 2.- Concluded.

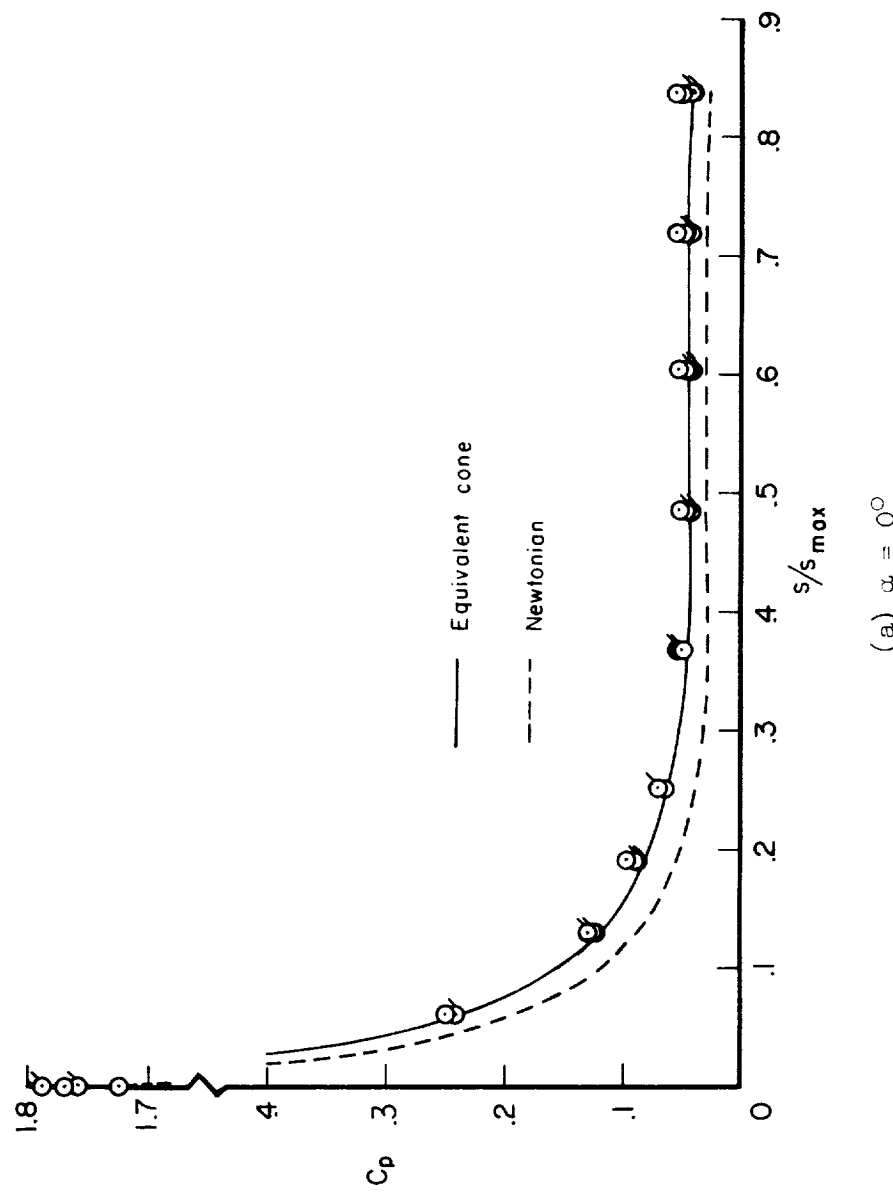
(a) $\alpha = 0^\circ$

Figure 3.- Local static-pressure distribution on most windward streamline.

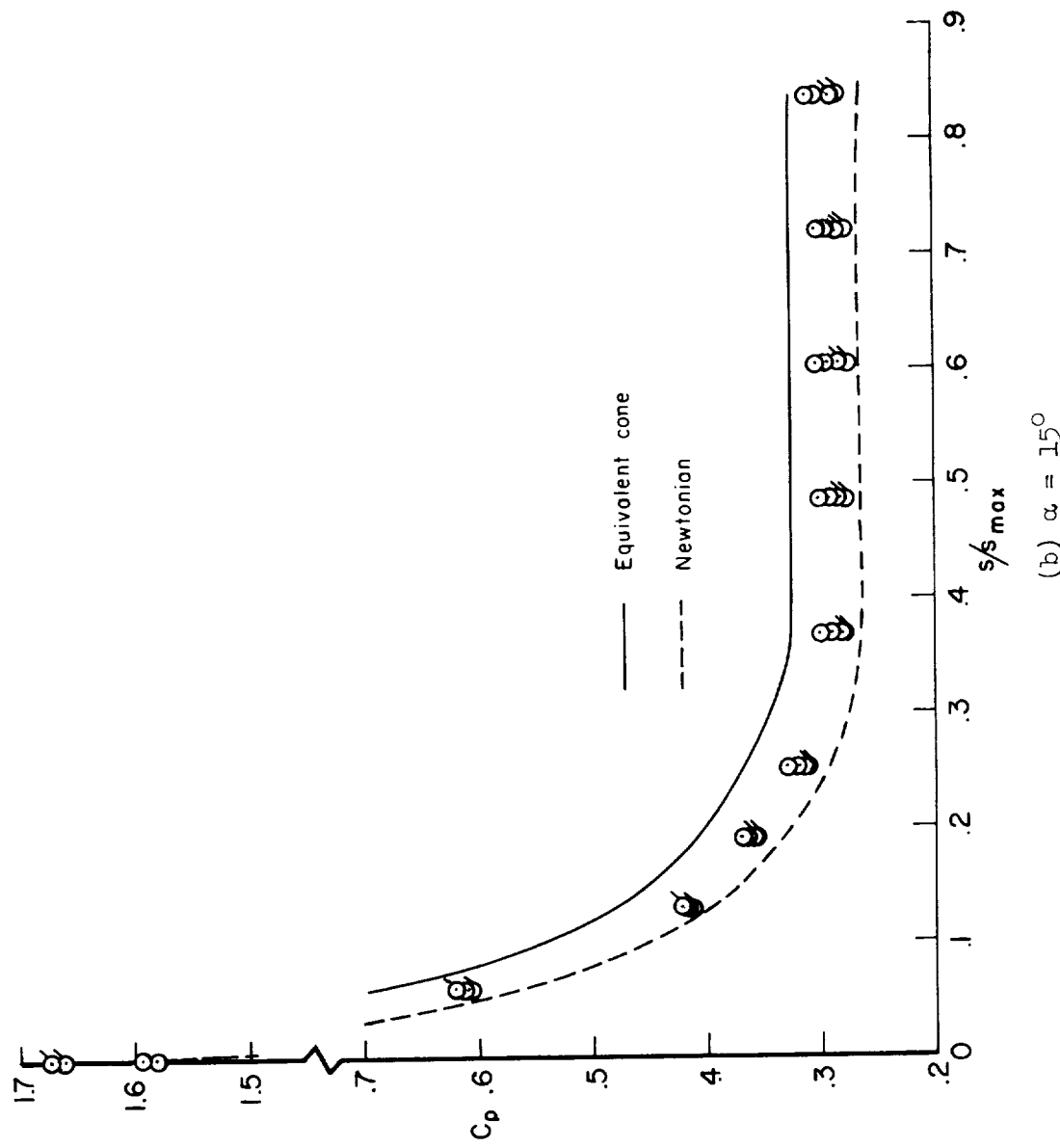


Figure 3.- Continued.
(b) $\alpha = 15^\circ$

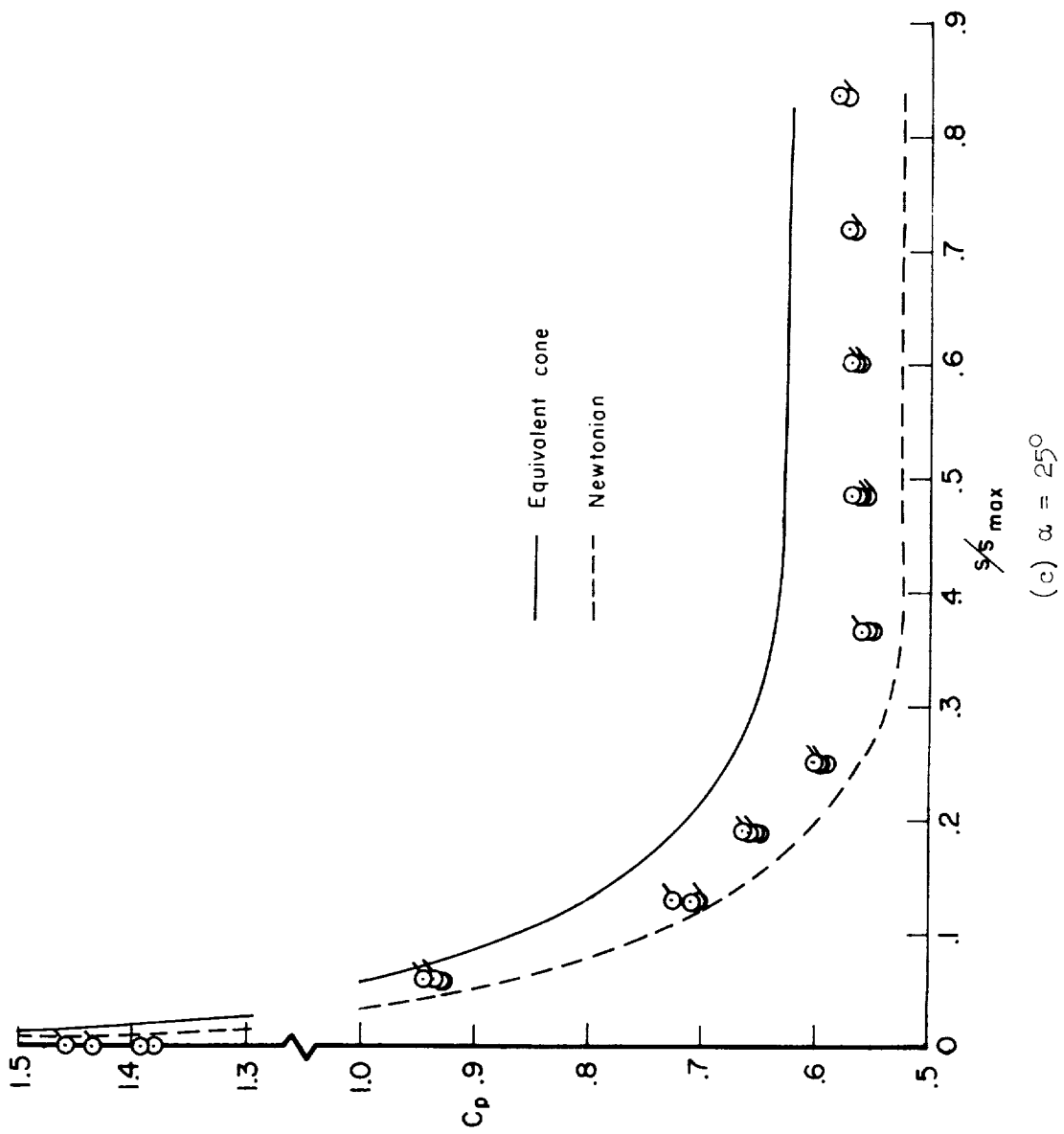


Figure 3.- Continued.
(c) $\alpha = 25^\circ$



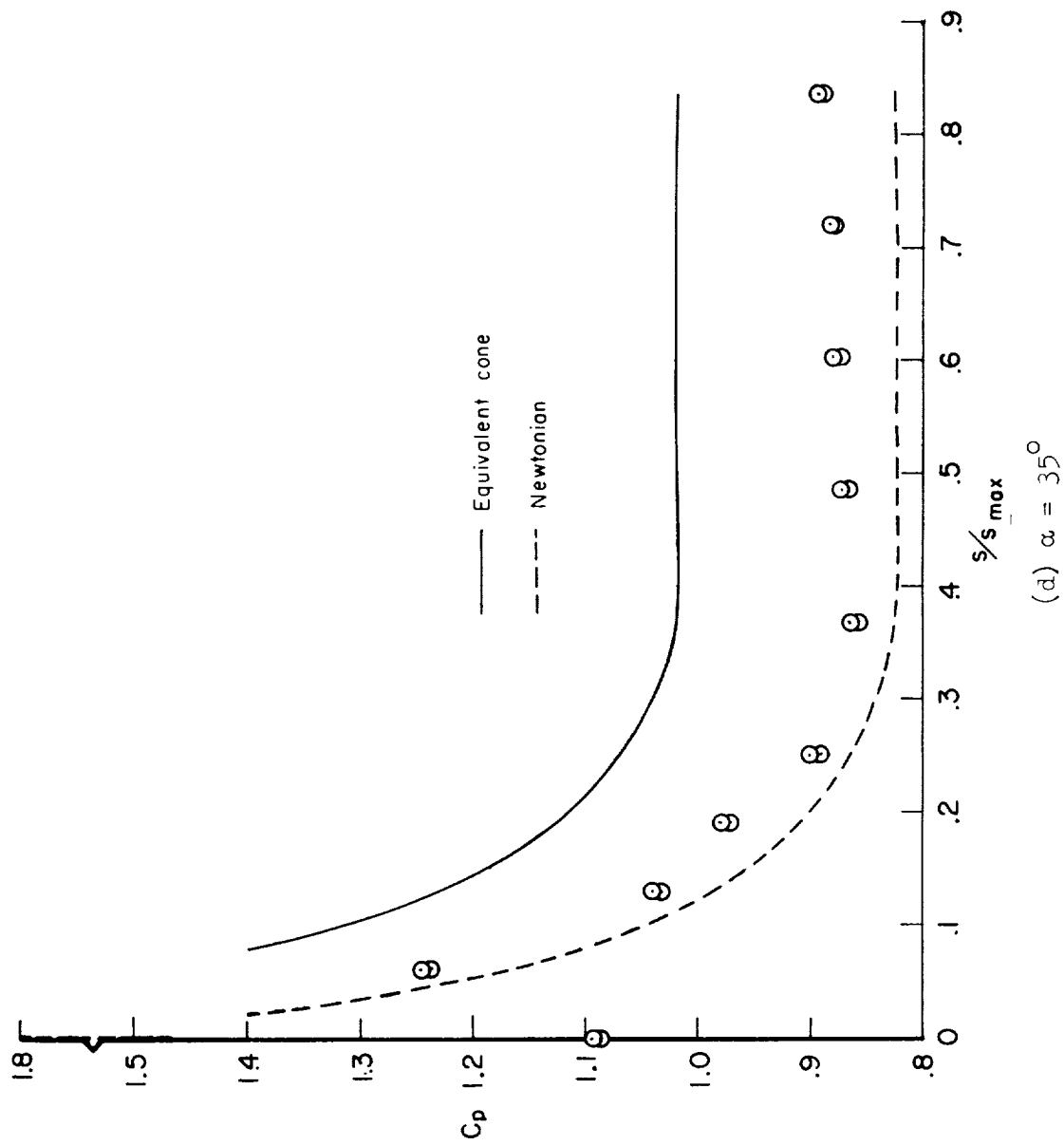


Figure 3. -- Concluded.



